Comparative Study of the Microstructure and Mechanical Properties of WC/High-Speed Steel Composite Materials Prepared with Co, Ni, and Fe Binders

HONGNAN LI,[1] HONGMEI ZHANG,[1,3] DEGE CHEN,[1]
and ZHENGYI JIANG[1,2,4]

1.—School of Materials and Metallurgy, University of Science and Technology Liaoning, Anshan 114051, China. 2.—School of Mechanical, Materials, Mechatronic and Biomedical Engineering, University of Wollongong, Wollongong, NSW 2522, Australia. 3.—e-mail: zhanghm@ustl.edu.cn. 4.—e-mail: jiang@uow.edu.au

Three-mm-diameter WC/HSS composites with different binders (Co and Co-Ni-Fe) were prepared. The effect of two different binders on the microstructure and properties of WC powder and HSS composites was compared to investigate the feasibility of substituting Fe and Ni for Co in WC and steel composites. The results show that the WC/HSS sample without binder has significant macropores at the interface, with a porosity of up to 43.76%. The porosity of the composite material containing Co binder is 6.07%. The partial substitution of Ni and Fe for Co significantly reduces the shrinkage temperature of WC powder, and the porosity was reduced to 0.77%. The addition of Ni and Fe in WC facilitates the mutual diffusion among Cr, Mo, and Co elements and the interface bonding between WC and HSS. After adding Ni and Fe elements, the microhardness of the WC/HSS composite materials is slightly lower than that of the Co-added composites, with a microhardness of 1204 HV in the WC region. The HSS microhardness remains almost constant during the binder substitution, maintaining around 600 HV. The wear resistance of the composite outer layer can be effectively enhanced by the use of Co, Ni, and Fe additives.

INTRODUCTION

Tungsten carbide (WC) is widely used in fields such as wear-resistant components, cutting tools, medical equipment, and electronic packaging.[1–3] Co is known to be traditionally used as a binder in the production of cemented carbide. However, Co is costly and resources are scarce, and it is necessary to consider both its harmfulness and the pollution caused by the environment.[4–6] Therefore, environmentally friendly cemented carbide with superior performance and low cost has become an essential research field. Among the Fe group metals, Fe and Ni are inexpensive, more environmentally friendly, and have preeminent wettability, making them the best alternatives to Co. Researchers have done a lot of work on WC-Fe-Ni-Co cemented carbides. Zhai et al.[7] demonstrated decent bonding performance with WC using CoCuFeNi medium entropy alloy binder instead of pure Co binder. The hardness and fracture toughness of the newly developed cemented carbide reached 1506.7 HV_{30} and 10.33 $MPa\cdot m^{1/2}$, respectively. Liu et al.[8] studied the effects of different binder compositions (including Co, FeNi, FeCoNi) on the hardness and toughness of WC cemented carbide. WC-20FeNi and WC-20FeCoNi cemented carbides exhibit higher toughness but lower hardness than WC-20Co cemented carbides. Chang et al.[9] studied the sintering properties of nano WC-15wt.% (Fe-Ni-Co) and WC-15wt.% Co, indicating that WC-(Fe-Ni-Co) alloys can be sintered at lower temperatures while still maintaining their excellent mechanical properties. The above studies indicate the great potential of Ni and Fe as

substitutes for Co. In addition, WC cemented carbides with Ni and Fe as substitutes for Co have been prepared by Chang et al.,[10] Soria-Xiurrun et al.,[11] and Shichalin et al.[12] by improving the device quality and adjusting the element ratios. Their results can achieve mechanical properties similar to those of WC-Co cemented carbides and even improve the toughness and corrosion resistance of WC cemented carbides. At present, most of the attention of scholars is focused on homogeneous WC cemented carbide materials, but the advantages of composite materials in being able to exert higher integrated properties cannot be neglected.

The problem of poor toughness of homogeneous WC cemented carbides still needs to be addressed effectively. Therefore, materials with higher strength can be used to fabricate structural parts with supporting effect. If WC cemented carbide is connected to steel, it will help combine the advantages of excellent wear resistance and good hardness with the extreme toughness and low price of steel, achieving the complementary advantages of the two materials and significantly increasing the utility of cemented carbide. Liu et al.[13] selected WC-Co particles as the reinforcing material and prepared GCr15 bearing steel matrix composite material through laser cladding technology. Zheng et al.[14] brazed WC-Co cemented carbide with 40Cr steel using Ag-41Cu-18In-6Ti alloy coating. Chen et al.[15] used Ni layer and resistance welding method to combine WC-10Co particles to B318 steel. Erfanmanesh et al.[16] used WC-Ni composite powder particles as on AISI 321 steel by laser cladding method. Scholars have used spark plasma sintering,[17,18] plasma spraying,[19] and welding[20–22] to achieve the joining of cemented carbide to steel. However, most of the existing studies have combined WC with steel by introducing interlayers and adding post-heating treatments, which are complex processes and mainly focus on the fabrication of large-sized WC/steel parts. In contrast, there is a growing demand for lightweight, thin, and miniaturized fine components as the industry advances, so the development of small-sized WC/steel composite materials is of great significance.

Jiang et al.[23] explored the effect of the brazing temperature and holding time on the interfacial properties of WC-Co/intermediate layer/35CrMo under high-frequency induced brazing. Jankauskas et al.[24] investigated the effects of WC particle size and WC content on the wear performance of WC and steel bonded materials. Li et al.[25] comprehensively evaluated the effect of WC particle on the phase composition, Vickers hardness, friction and wear properties, and tensile properties of laser melt deposited 316L. Cheniti et al.[26] investigated the effects of different brazing currents on the diffusion, bonding strength, and interface hardness of WC-Co carbide/1020 steel prepared. Avettand Fènoël et al.[27] explored the wear properties of Ni interlayer at steel-ceramic interface with different thicknesses. Nowadays, researchers have investigated the influence of various parameters including the intermediate layer, WC particle size, WC content, temperature, and holding time on the properties of WC and steel. These studies provide guidance on the effects of various experimental parameters, microstructure analysis, and bonding mechanics. However, there is still little research on the effect of changes in the type of binder on the connection between cemented carbide and steel during binder substitution. Interfacial stability, microstructural characteristics, and mechanical properties during binder substitution of WC and steel composite materials remain a scope of research. Furthermore, to the best of our knowledge, there is no literature exploring the effect of Ni and Fe replacing Co on the bonding properties between WC cemented carbides and steel.

In this work, small-sized WC-Co-Ni-Fe/high-speed steel (HSS) composites of 3 mm diameter were successfully prepared after partial replacement of Co by Ni and Fe. The feasibility of replacing Co binder with Ni and Fe for the diffusion bonding of WC to steel was investigated by comparing the microstructure, interface stability, and mechanical properties of WC/HSS, WC-Co/HSS, and WC-Co-Ni-Fe/HSS composites.

EXPERIMENTAL PROCEDURES

Raw Materials

High-purity WC, Co, Ni, and Fe powders (morphology and particle size distribution are shown in Fig. 1) and high-speed steel (HSS) bar (d = 1 mm) are used as raw materials.

Preparation of Composite Materials

The experimental procedure for preparing the WC/HSS composite is shown in Fig. 1.

a   First, the binder addition was optimized through comparative experiments. The compositions used in the binder optimization process for the WC/HSS composites are listed in Table I. The interface microstructure of WC/HSS with different binder compositions is shown in Fig. 2. Figure 2 indicates the interface bonding effect is better when the proportion of binder is 40% and the ratio of Co, Ni, and Fe is 2:1:1. Therefore, WC and Co mass ratio of 6:4 and WC, Co, Ni and Fe powder mass ratio of 6:2:1:1 were used, and the powders were proportionally weighed using an electronic balance.

b   A planetary ball mill was used to mix the powder. The powder is milled by a ball mill at a rate of 200 r/min for 1 h, with the rotation direction switched at 30 min to ensure uniform powder mixing.

c   The mixture of powder and steel is loaded into a self-made mold (310 s stainless steel) to make a composite material green-pressing with a diam-
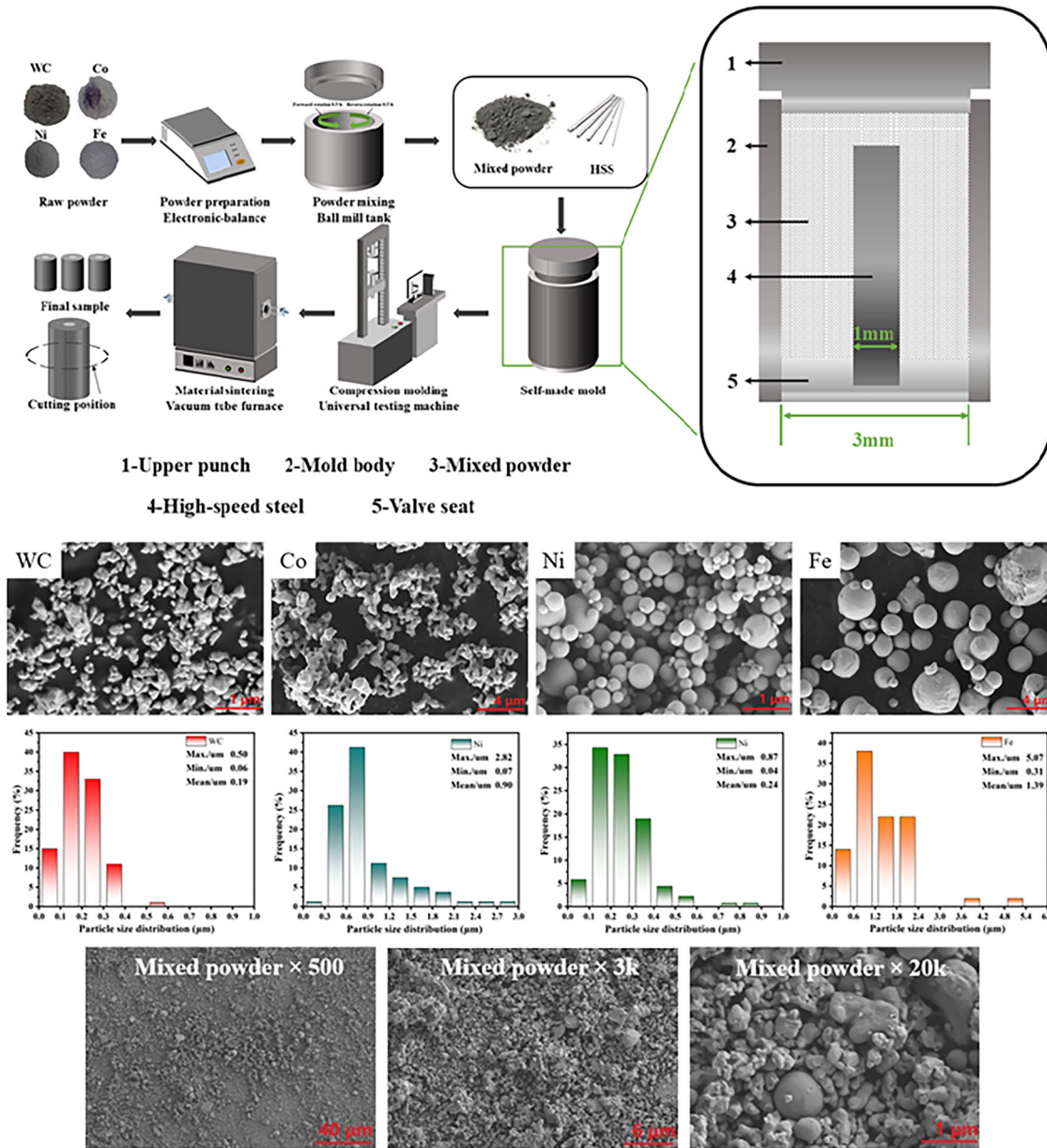
Fig. 1. Experimental process for preparation of WC (powder)/HSS (solid bar) composite materials.

Table I. Composition of WC/high-speed steel with different binder ratios

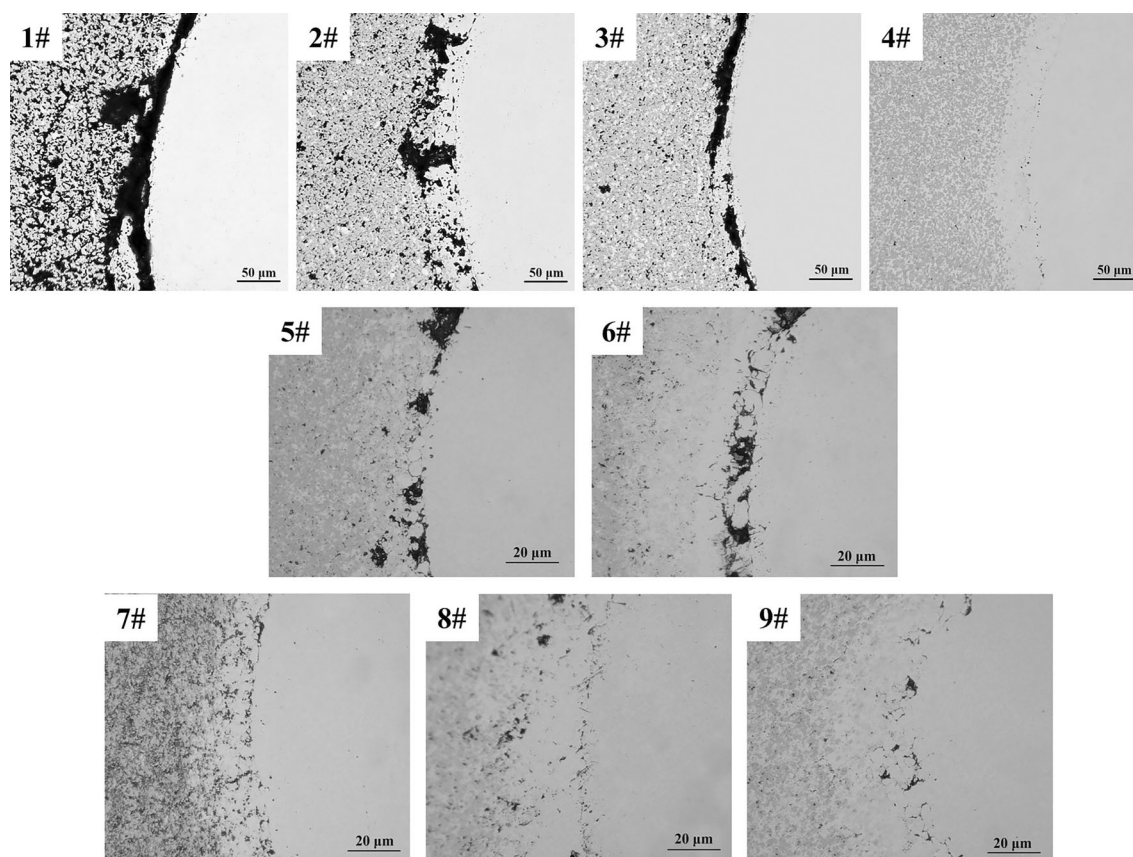| Sample numbers	WC content (ω/%)	Binder content (ω/%)	Binder content (mass ratio)		
			Co	Ni	Fe
1#	90	10	2	1	1
2#	80	20	2	1	1
3#	70	30	2	1	1
4#	60	40	2	1	1
5#	60	40	0	2	2
6#	60	40	2	2	0
7#	60	40	2	0	2
8#	60	40	1	2	1
9#	60	40	1	1	2

Fig. 2. Microstructure of WC/HSS with different binder compositions.

eter of 3 mm. The mold consists of an upper punch, a mold body, and a valve seat.

d   The powder was compressed at an average pressure of 1000 MPa for 10 s using a universal test machine (Jinan Chenda Testing Machine Manufacturing Co., Ltd., WDW-300, Zhong Lu Chang, Jinan, China). The loading rate was set to 5 mm/min.

e   The sample was sintered in a vacuum tube furnace. The sintering temperature is set to 1280°C, the heating rate of the vacuum tube furnace was set at 6°C/min, the holding time is set to 90 min, and finally it cools down with the furnace.

f   A NC linear cutting machine (SMDK-320 T, Taizhou Jinggong Electromechanical Manufacturing Co., Ltd, China) was used to cut the middle of the sample to obtain the detection cross section, and a polishing machine was used to polish it. After cutting and polishing, the sintered samples were tested for microstructure and performance.

Microstructure and Properties Analyses

The microstructure of the WC region and the interfacial microstructure of the composite were examined using super depth of field microscope

(VHX-5000, Keyence (China) Co., Ltd., Shanghai, China) and SEM (Zeiss-IGMA HD, Jena, Germany). Energy-dispersive spectroscopy (EDS Zeiss-IGMA HD, Jena, Germany) is used to detect the distribution of elements at the interface of composite materials. A thermal expansion coefficient tester [DIL 402 Expedis Classic, NETZSCH Scientific Instrument Trading (Shanghai) Co., Ltd., China] was used to measure the coefficient of thermal expansion of the powder. Image J software (National Institutes of Health, Bethesda, MD, USA) was used to analyze the surface porosity in the WC region based on images of microstructures taken under digital microscopy. The microhardness of the composite was determined using a micro-hardness tester (Q10M, Qness GmbH, Salzburg, Austria). The wear performance of the composites was tested and evaluated using a ball-disc friction and wear tester (MS-T300, Lanzhou Huahui Instrument Technology Co., Ltd, Lanzhou, China) at room temperature under dry and lubrication-free conditions. The friction counterpart was a zirconia ball, the load was set at 10 N, the rotational speed was set at 200 r/min, and the wear time was set at 120 min. Laser confocal microscopy (VL2000DX, Yonekura MFG Co., Ltd., Japan) was used to observe the interface microstructure of composite materials during heating.

RESULTS AND DISCUSSION

Coefficient of Thermal Expansion of WC Powder Under Different Binders

To investigate the effect of Co-Ni-Fe additive on the shrinkage of WC powder during the sintering process, or the changes in WC powder shrinkage caused by Ni and Fe elements replacing Co elements, the thermal expansion rate curves of WC, WC-Co, and WC-Co-Ni-Fe powder systems in a vacuum environment within the sintering temperature range of 25–1280°C were measured, as shown in Fig. 3. The three materials have almost no expansion phenomenon before the temperature of 25–500°C, and the expansion behavior occurs at 500°C. Between 500 and 700°C, the three materials rapidly expand. At 700–900°C, the expansion rate of WC and WC-Co materials increases slowly, but the expansion rate of WC-Co-Ni-Fe materials still increases rapidly; the maximum thermal expansion rate is about 52.7×10^{-3} at 842°C. The expansion of WC and WC-Co powders increases slowly when the temperature exceeds 900 °C. The WC powders are still expanding at the cut-off temperature, and the thermal expansion of WC-Co reaches a maximum of 44.4×10^{-3} at 1085 °C and then decreases with increasing temperature. The thermal expansion of WC-Co-Ni-Fe decreases rapidly with increasing temperature after 842 °C. The thermal expansion of WC-Co-Ni-Fe decreases rapidly with increasing temperature because the thermal motions and interactions of the elements Co, Ni, and Fe change or even undergo a phase transition at this temperature, which leads to a weakening of the expansion tendency of Co, Ni, and Fe. The WC-Co-Ni-Fe thermal expansion is negative at a temperature of about 981 °C. This temperature is close to the sintering temperature of the liquid phase. A thermal expansion rate of less than zero indicates that the object shrinks or shrinks faster than it expands at elevated temperatures. Soria Bairrun et al.[28] analyzed that the shrinkage phenomenon may be related to the diffusion of Fe, Ni, and Co atoms toward the surface of WC grains. The mutual dissociation of Fe, Ni, and Co atoms changes the atomic diffusion rate during heating. Moreover, the thermal expansion rate of pure WC is very small compared to WC-Co and WC-Co-Ni-Fe with additives. As a result, its thermal stability is also higher than that of WC powder with binders. However, the better thermal stability does not favor the shrinkage of the powder. The addition of Co only causes a tendency for the thermal expansion of the WC powder to start decreasing after 1200 °C. The WC-Co-Ni-Fe powder is already shrinking from 981 °C. In contrast, WC-Co-Ni-Fe already shrinks at 981 °C. Therefore, the addition of Ni and Fe significantly reduces the temperature at which the WC alloy starts to shrink. The WC-Co-Ni-Fe alloy has sufficient time and temperature to shrink, which helps to reduce the porosity of the WC alloy.
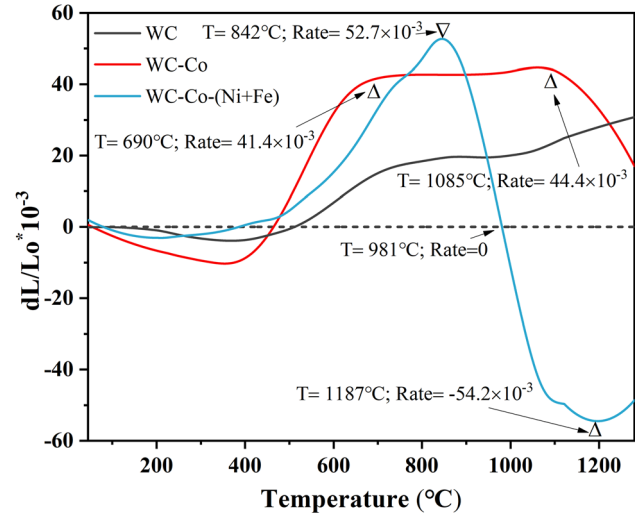

Fig. 3. Thermal expansion rate curves of WC, WC-Co, and WC-Co-Ni-Fe powder systems.

Furthermore, the thermal expansion rate of the WC-Co material is larger throughout the entire heating stage, while the thermal expansion rate of the WC-Co Ni-Fe material is larger only for a short period of time, and the size change of the WC-Co-Ni-Fe material has stabilized during the heating process. When the material is in the cooling process after sintering, the size change of the WC-Co material will be more significant compared to the WC-Co-Ni-Fe material.[29,30] The effect of thermal residual stress on WC-Co-Ni-Fe material is probably smaller compared to WC-Co material. Thus, replacing some of the Co by Ni and Fe is more favorable for WC powder contraction and porosity reduction.

Comparison of Ni-Fe Substitution with Co Porosity

The porosity in cemented carbides commonly reduces the mechanical properties of the material. If there are large pores in the highly stressed part of the specimen, it will result in a lower strength value before fracture.[31] Romanova et al.[32] indicated that the presence of residual pores reduces the transverse fracture strength of the material. Consequently, the size of porosity is an important criterion for evaluating the properties of cemented carbides. Figure 4 exhibits the microstructure and surface porosity measurements of the WC zone in the WC/HSS composite with different binders. The sample porosity collection method is shown in Fig. 4a. The surface porosity of the sintered sample gradually increases with Ni-Fe substitution for Co. Figure 4c shows the microstructure of the WC zone of the WC/HSS composite material. Pure WC powder has a large amount of non-density microstructure at a sintering temperature of 1280°C and is simply mechanically bonded. Lower density raw

cracks originating from the nano-powder pressing can also be observed in the WC zone. The surface average porosity of the WC region in WC/HSS is as high as 43.76%. With surface average porosity of up to 43.76% in the WC region of WC/HSS, it is reasonable to assume that at 1280 °C WC is in the solid phase sintering stage, where the movement of the powder particles is difficult because of the absence of the liquid phase and the presence of a large number of pores and holes in the sintered body. The melting point of pure WC is as high as 2800 °C and it is difficult to prepare binder-free WC carbide by conventional sintering processes. As shown in Fig. 4d, WC-Co powder has partially non-dense structure, many irregular pores, and uneven distribution. The surface average porosity was reduced to 6.07%. As shown in Fig. 4e, compared to WC-Co, the pores in WC-Co-Ni-Fe/HSS have a more spherical shape and a smaller aspect ratio, resulting in a more uniform stress distribution. In addition, the average surface porosity of the WC zone in WC-Co-Ni-Fe/HSS is as low as 0.77%. This is due to the addition of Ni and Fe, and the binder in the WC zone forms a liquid phase. Under the action of the capillary force, the liquid phase fills the pores and penetrates between the solid particles in the WC matrix, accompanied by the rearrangement of the WC particles and the dissolution and precipitation in the liquid phase, filling the porous region and increasing the density. In addition, the addition of Ni and Fe increases the liquid-phase reaction between WC and Co, thus providing more particle contact area and increasing the solid-phase diffusion rate between particles. This will enhance the sintering driving force.[33] Therefore, denser microstructures can be obtained in the WC-Co-Ni-Fe zone at relatively low sintering temperatures.

Comparison of Interface Microstructure and Element Diffusion

The images of the cross-sectional microstructure and interface microstructure at 500 × magnification for the WC/HSS, WC-Co/HSS, and WC-Co-Ni-Fe/HSS composite materials are shown in Fig. 5. The microstructure of three types of composite materials can be classified as: HSS zone, bonded interface zone, and WC zone. Figure 5a shows the cross-sectional microstructure image of WC/HSS composite material, and the separation interface between the WC and HSS regions can be distinctly observed. There are distinct cracks at the interface and practically no connected interfaces. There are large cracks and powder fragments in the WC zone. At a magnification of 500 ×, there is a large amount of non-dense structure in the WC region, and there is no connection between the WC and the steel. Figure 5b and c shows cross-sectional microstructure images of WC-Co/HSS composite material and WC-Co-Ni-Fe/HSS composite material. The interfaces of the two composite materials

are in excellent connectivity, and no significant defects are observed in the microstructure of the WC zone. The powder is dense, and the interface is complete. Comparing the interface microstructure of the two materials after 500 × magnification, the interface formed by WC powder with Co additive and HSS exhibits large cracks and minor pores compared to the interface formed by WC powder with Co, Ni, and Fe binders. The overall surface of the WC-Co-Ni-Fe/HSS composite is flat, and the interface junctions are intact. Comparing all three materials shows that the Ni and Fe additives not only make the WC structure dense but also promote the diffusion and bonding of WC with high-speed steel.

The need to investigate the interfacial failure temperature of composites arises from the conversion of mechanical energy into internal energy during friction, which increases the temperature of the object and therefore may have an effect on the composite interface. Figure 6 shows the interfacial microstructure of the composite during the heating process. At about 680°C, the interface of WC-Co/HSS composite material begins to melt. The melting of the interface at 680°C is mainly due to differences in material melting points. WC and steel have different melting points. In high-temperature environments, the melting point of steel is lower than that of WC, which may lead to partial melting of steel at 680°C. The interface melting intensifies at 1025°C. The interface remains connected at 1350°C. WC-Co-Ni-Fe/HSS has little change at the interface until 1025 °C; between 1025-1350 °C the interface melts violently, and at 1350 °C the interface fails completely. Thus, the substitution of some Co elements by Ni and Fe raises the initial melting temperature of the interface and decreases the interface failure temperature.

The images of the microstructure and EDS surface scan distribution of elements at the interface between WC-Co/high-speed steel and WC-Co-Ni-Fe/high-speed steel composite materials are shown in Fig. 7. Depending on the microstructure, the diffusion of the composite material can be divided into two types: diffusion from the WC region to the high-speed steel region and diffusion from the high-speed steel to the WC side. In this study, the major elements with higher content are mainly studied, including W, Co, and Ni elements in the WC region and Fe, Mo, and Cr elements in the high-speed steel region. Other elements had lower content and diffusion and were not observed in this study. As Fig. 7a shows, in the pure WC zone, a dense layer of about 20 μm Fe is formed at the interface, and large cracks appear near the dense layer, which is attributed to the fact that no liquid phase is formed in the pure WC zone at 1280°C, and the WC is poorly dense, with a large amount of non-dense tissue, which prevents the diffusion of elements from the HSS to the WC zone. The diffusion of Mo and Cr elements from the HSS zone to the WC zone
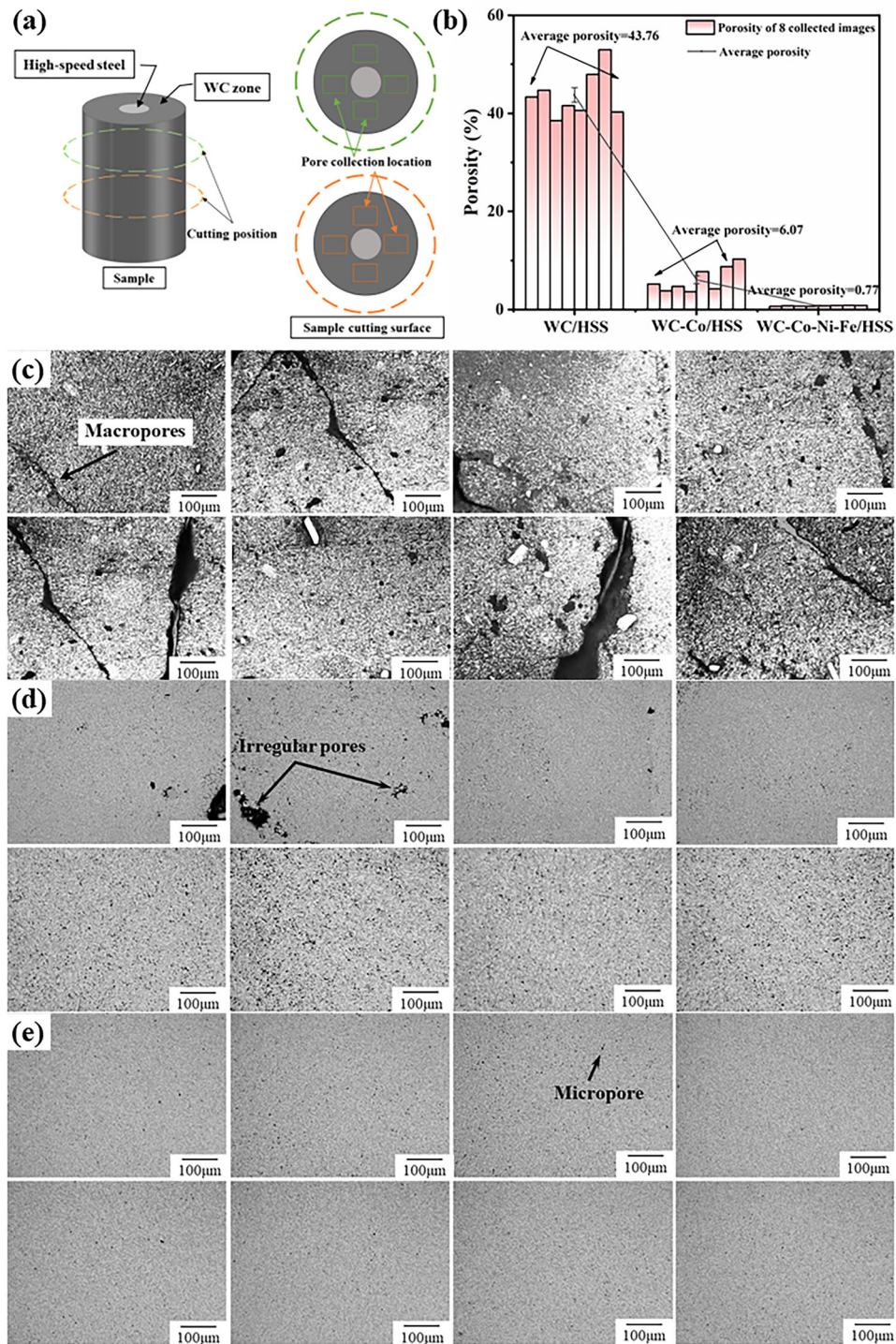
Fig. 4. Microstructure and porosity of WC zone in WC/high-speed steel composite materials: (a) schematic diagram of pore collection; (b) porosity; (c) WC; (d) WC-Co; (e) WC-Co-Ni-Fe.

decreases as the diffusion distance increases. As shown in Fig. 7b, for the WC-Co/HSS composite, the Fe, Cr, and Mo elements in the HSS all diffuse into the WC zone, and the Co elements diffuse into the HSS, where it can be found that the Fe, Cr, and Mo elements mainly diffuse into the Co additive zone. Adding Co to the WC particles increases the

diffusion of Fe, Cr, and Mo elements from the HSS to the WC zone, decreasing the cracking at the composite interface and improving the quality of the interfacial bonding of the composite. As shown in Fig. 7c, the WC interface is strongly bonded, and there are uniform micropores at the interface. This is due to the different diffusion rates of the
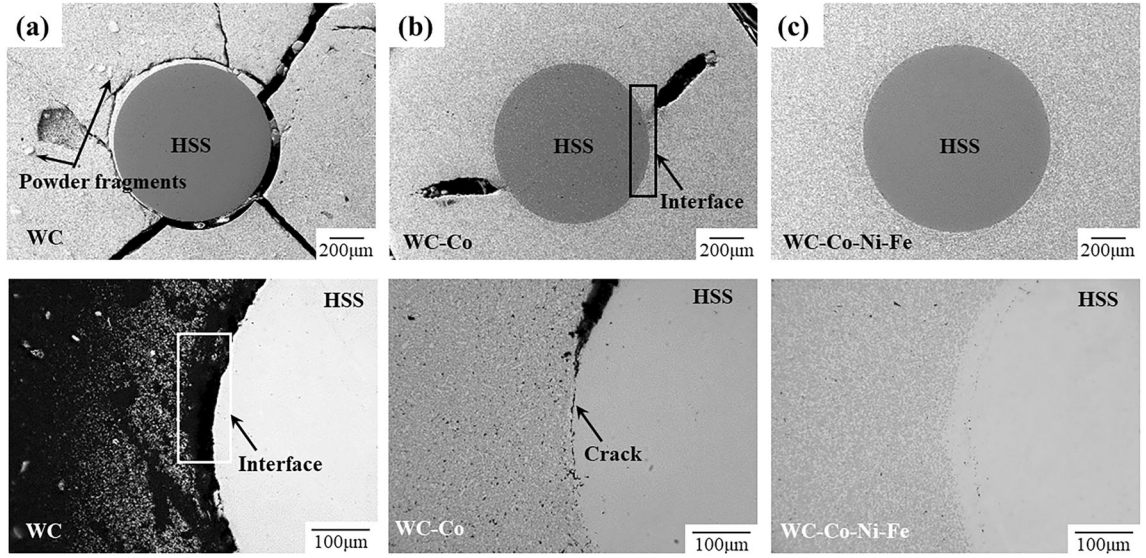
Fig. 5. Interface microstructure of three composite materials.
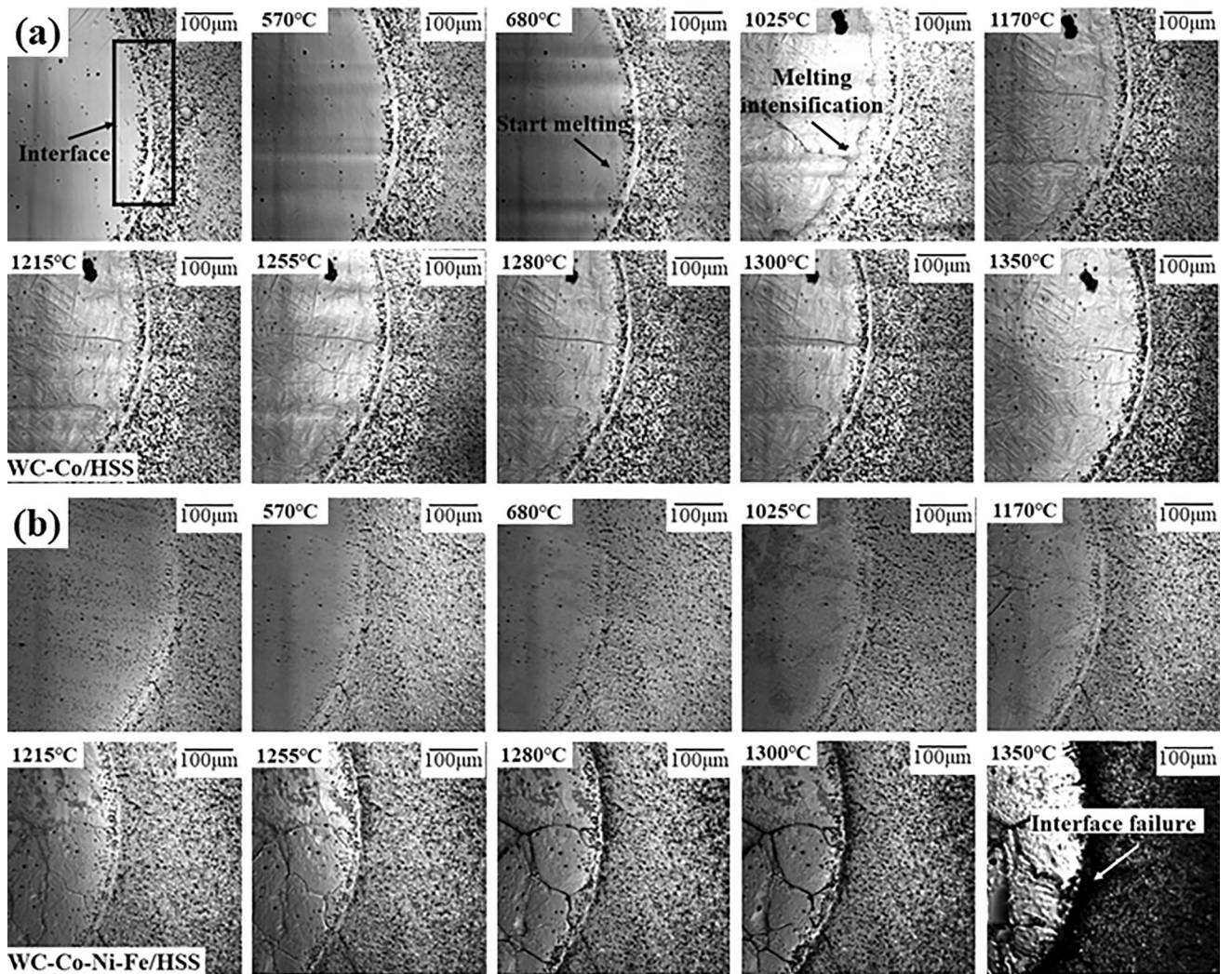

Fig. 6. Interface of WC/HSS composite material during heating process: (a) WC-Co/HSS; (b) WC-Co-Ni-Fe/HSS.

elements, which leads to the formation of vacancy defects during the element diffusion process, causing this phenomenon. The number of these vacancy defects increases and gradually aggregates to form holes, and the micropores at the interface are tentatively identified as Kirkendall micropores. As observed from the scan images, the degree of element diffusion in the WC-Co-Ni-Fe/HSS composite materials is more pronounced compared to the WC-Co/HSS composite materials, with the Co and Ni elements being more pronounced, which can indicate that the addition of Ni and Fe elements to the WC contributes to the interdiffusion of the elements and further proves that the addition of Fe and Ni accelerates element diffusion. This is in addition to the fact that the degree of diffusion of Co elements is more pronounced than for Ni, Mo, and Cr elements throughout the composite. Since diffusive transport of elements is strongly motivated by differences in the concentration of elements in different types of materials, in the WC-Co-Ni-Fe and HSS zones, the Co element has a larger concentration gradient compared to Ni, Mo, and Cr. In addition, no significant diffusion of W elements is found in the HSS region of any of the three composite materials because of the high molecular weight of W, which does not diffuse easily into the HSS. As described by Refs. [34–37], diffusion is related to the atomic size of the alloying elements in the composite materials. In summary, the addition of Co, Ni, and Fe contributes to the diffusion bonding of WC to HSS, where the possibility of Ni and Fe replacing Co from an elemental diffusion perspective is demonstrated.

Comparison of Microhardness

Figure 8 displays the cross-sectional microhardness of the WC-Co/HSS and WC-Co-Ni-Fe/HSS composite materials. We can see clearly that the microhardness in the WC region is significantly higher, with hardness values > 1000 HV, compared to high-speed steel. The hardness values in the WC region near the high-speed steel region are slightly higher than those in the WC region on either side. This phenomenon is attributed to the possible presence of large-sized WC and brittle hard phases in the interface structure. The microhardness values of high-speed steel are maintained at around 600 HV, which is nearly the same as the Vickers hardness of high-speed steel at different temperatures studied by Lee et al.,[38] indicating that there is no loss or increase in steel hardness during the sintering process. The maximum microhardness value of WC-Co/HSS composite material is 1324 HV. The main cause of that is that higher Co addition reduces the W content per unit area in the WC region and reduces the hardness of the WC tissue. In addition, low fluctuations in the microscopic hardness are observed in the WC/HSS sample, indicating that the WC is well distributed in the

microstructure and has a homogeneous structure. The hardness values of the WC-Co/HSS composite materials reach up to 1204 HV, and the microhardness of the WC-Co-Ni-Fe region is slightly lower compared to the WC-Co region, a result consistent with the findings of Qian et al.,[39] who also obtained a higher hardness for the WC-Co cemented carbide than for the WC-CoNiFe cemented carbide with the same WC powder particle size. The reason for the lower hardness values may be the presence of Ni and Fe. Co has a high solid solubility and forms uniform and fine carbide phases, resulting in a higher hardness. However, the low solid solubility of Ni and Fe makes it difficult to efficiently form the carbide phase, thus reducing their hardness.

Comparison of Wear Rate

Due to the low density of pure WC/HSS composites, the hardness and wear were not compared with WC-Co/HSS and WC-Co-Ni-Fe/HSS. The wear profile curves and wear rate histograms for the composite WC-Co, WC-Co-Ni-Fe, and HSS regions under a 10 N load are shown in Fig. 9. The depth and width of the wear marks are larger for WC-Co than for WC-Co-Ni-Fe and are maximum for HSS. For WC-Co, the width of the wear marks is about 260 μm, the depth of the wear marks is about 4.5 μm, and the wear rate is 7.1×10^{-5} mm^3/Nm; for WC-Co-Ni-Fe, the width of the wear marks is about 210 μm, the depth of the wear marks is about 2.8 μm, and the wear rate is 4.1×10^{-5} mm^3/Nm. For HSS, the abrasion width is about 430 μm, the depth is about 15 μm, and the wear rate is 42×10^{-5} mm^3/Nm. The application of the WC layer results in a dramatic reduction in the variation and wear rate of the wear profile. WC-Co-Ni-Fe has the smallest wear rate, indicating the best resistance compared to WC-Co and HSS. Where for both WC-Co-Ni-Fe and WC-Co material surface porosity and microhardness can be seen where WC-Co-Ni-Fe has a higher density and WC-Co a higher hardness, compared to the relatively higher hardness and higher density, the higher density plays a greater role in wear resistance, giving it a higher load-bearing capacity and thus showing a higher resistance to wear. Although the hardness of WC-Co-Ni-Fe is slightly reduced compared to WC-Co, its excellent bonding properties play an essential role in the great wear resistance it exhibits. In contrast, the sparser WC structure of WC-Co makes it less resistant to abrasion. Thus, the results show that the use of WC and additives can effectively enhance the wear resistance of the outer layer of the composite, along with the Ni and Fe addition, which can effectively enhance the WC wear resistance.

CONCLUSION

The effects of the addition of Co, Ni, and Fe binders on the porosity, interfacial microstructure, diffusion of interfacial elements, microhardness,
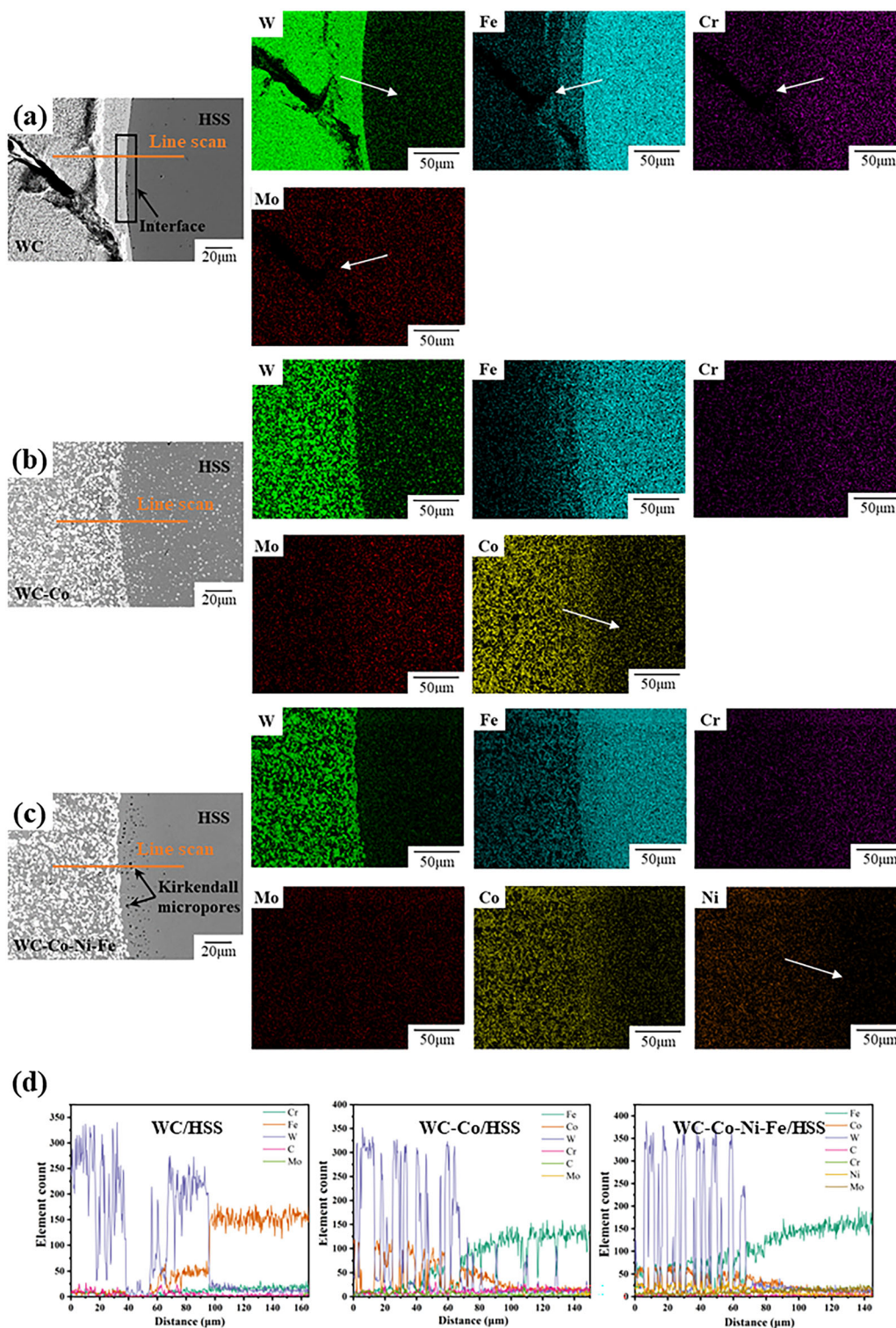
Fig. 7. Scanning element diagrams of interface surfaces of three composite materials: (a) pure WC without additives; (b) adding Co elements; (c) adding Co, Ni and Fe elements; (d) line scan diagram.

and wear of WC/HSS were compared. Based on the obtained data, the following conclusions can be drawn.

a. The porosity in the binder-free WC region is relatively high, and the WC/HSS composite exhibits a significant large porosity at the interface. A useful metallurgical bond cannot be obtained. The composite addition of Ni, Fe, and Co significantly reduces the WC density temperature, which promotes not only the den-
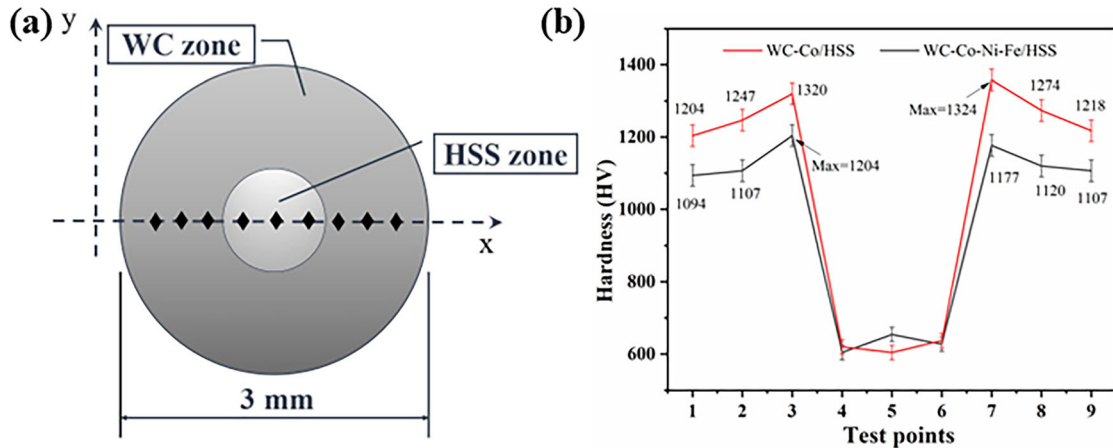
Fig. 8. Microhardness curve of WC/HSS composite material: (a) measurement points; (b) microhardness curves.
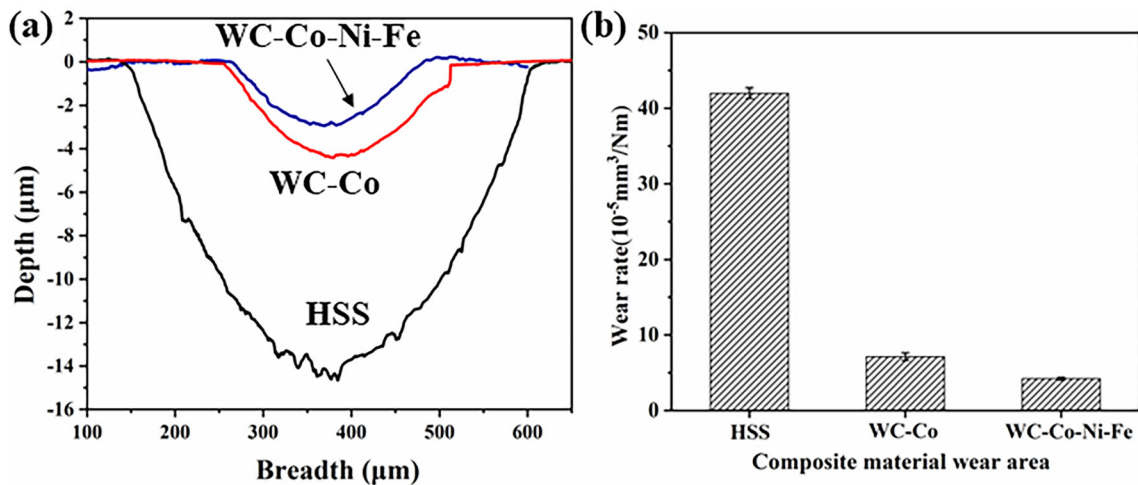

Fig. 9. Wear diagram of WC/HSS composite material: (a) wear morphology; (b) wear rate.

sification of the WC region, but also the connection of WC powder with high-speed steel.

b. The addition of Ni and Fe to WC contributes to the mutual diffusion of Cr, Mo, and Co elements, but no significant diffusion of W elements is found in any of the three composite materials.

c. Comparing the microhardness of the WC-Co/HSS and WC-Co-Ni-Fe/HSS composite materials, the addition of Ni and Fe elements slightly reduces the microhardness in the WC region, but the value of the microhardness in the HSS region does not change significantly because of the binder changes.

d. The WC side wear rate of the WC/HSS composites with Co-Ni-Fe addition is lower than that of the WC/HSS composites with only Co addition. Ni and Fe partially replace Co elements to improve the wear resistance of WC/HSS.

e. The replacement of Co by Ni and Fe in WC tungsten carbide slightly reduces hardness and

wear resistance. However, the replacement of a portion of Co by Ni and Fe not only saves the consumption of scarce Co resources but also improves the quality of the interfacial connection between WC and steel composites, which has a more important impact on the production cost, durability, and lifetime of the composites. Therefore, Ni and Fe substitutions of some Co are promising for WC/HSS composites.

FUNDING

CONFLICT OF INTEREST

On behalf of all authors, the corresponding author states that there is no conflict of interest.

REFERENCES

1. I. Konyashin, S. Hlawatschek, B. Ries, F. Lachmann, and M. Vukovic, *Int. J. Refract. Met. H.* 42, 142 https://doi.org/10.1016/j.ijrmhm.2013.08.016 (2014).

2. J. Gurland, and P. Bardzil, *Jom.* 7, 311 https://doi.org/10.1007/BF03377497 (1955).

3. Y. Yang, C. Zhang, D. Wang, L. Nie, D. Wellmann, and Y. Tian, *Int. J. Adv. Manuf. Tech.* 108, 1653 https://doi.org/10.1007/s00170-020-05389-5 (2020).

4. N. Ku, J.J. Pittari III., S. Kilczewski, and A. Kudzal, *Jom.* 71, 1535 https://doi.org/10.1007/s11837-019-03366-2 (2019).

5. T. Soria-Biurrun, J.M. Sánchez-Moreno, and K. Frisk, *Int. J. Refract. Met. H.* https://doi.org/10.1016/j.ijrmhm.2021.105719 (2022).

6. P. Pereira, A.F. Rocha, J. Sacramento, F.J. Oliveira, L.F. Malheiros, A.M.R. Senos, and A.C. Bastos, *Int. J. Refract. Met. H.* https://doi.org/10.1016/j.ijrmhm.2022.106019 (2023).

7. K. Zhai, S. Chen, C. Wang, Q. Li, B. Sun, and J. He, *Int. J. Refract. Met. H.* https://doi.org/10.1016/j.ijrmhm.2022.105808 (2022).

8. C. Liu, Alternative binder phases for WC cemented carbides, Master Thesis, KTH, Stockholm (2014).

9. S.H. Chang, M.H. Chang, and K.T. Huang, *J. Alloy. Compd.* 649, 89 https://doi.org/10.1016/j.jallcom.2015.07.119 (2015).

10. S.H. Chang, and S.L. Chen, *J. Alloy. Compd.* https://doi.org/10.1016/j.jallcom.2013.09.188 (2014).

11. T. Soria-Biurrun, L. Lozada-Cabezas, J. Navarrete-Cuadrado, F. Ibarreta-Lopez, R. Martinez-Pampliega, and J.M. Sanchez-Moreno, *Int. J. Refract. Met. H.* https://doi.org/10.1016/j.ijrmhm.2022.105994 (2023).

12. O.O. Shichalin, I.Y. Buravlev, A.S. Portnyagin, M.I. Dvornik, E.A. Mikhailenko, A.V. Golub, and E.K. Papynov, *J. Alloy. Compd.* https://doi.org/10.1016/j.jallcom.2019.152547 (2020).

13. S. Liu, Y. Li, Y. Wang, Y. Wei, L. Zhang, and J. Wang, High wear resistance WC-Co reinforced GCr15 bearing steel composite prepared via selective laser melting (SLM). *Int. J. Refract. Met. H.* https://doi.org/10.1016/j.ijrmhm.2022.105988 (2022).

14. Z. Zheng, S. Shao, M. Xu, R. Ma, A. Du, Y. Fan, and X. Cao, *Int. J. Refract. Met. H.* https://doi.org/10.1016/j.ijrmhm.2022.106092 (2023).

15. L. Chen, C. Zhang, Z. Guo, and G. Liu, *Int. J. Refract. Met. H.* https://doi.org/10.1016/j.ijrmhm.2023.106221 (2023).

16. M. Erfanmanesh, H. Abdollah-Pour, H. Mohammadian-Semnani, and R. Shoja-Razavi, *Opt. Laser Technol.* 97, 180 https://doi.org/10.1016/j.optlastec.2017.06.026 (2017).

17. M. Hasan, Z. Huang, J. Zhao, A. Jumlat, F. Jia, H. Wu, and Z. Jiang, *Int. J. Adv. Manuf. Tech.* 111, 2405 https://doi.org/10.1007/s00170-020-06210-z (2020).

18. J.T. Cahill, J.P. Kelly, E. Novitskaya, M. McKee, J.A. Bahena, and O.A. Graeve, *J. Am. Ceram. Soc.* 102, 595 https://doi.org/10.1111/jace.15814 (2019).

19. Y.C. Zhao, Y. He, J. Zhang, C. Meng, X. Zhang, and S. Zhang, *Surf. Coat. Technol.* https://doi.org/10.1016/j.surfcoat.2022.129049 (2023).

20. L. Chen, Z. Guo, C. Zhang, Y. Li, C. Wu, and G. Liu, *Ceram. Int.* 47, 17400 https://doi.org/10.1016/j.ceramint.2021.03.056 (2021).

21. M. Nagentrau, A.M. Tobi, M. Sambu, and S. Jamian, *Int. J. Refract. Met. H.* 82, 43 https://doi.org/10.1016/j.ijrmhm.2019.03.029 (2019).

22. C. Wu, C. Guo, G. Liu, Y. Li, and L. Chen, *Int. J. Refract. Met. H.* https://doi.org/10.1016/j.ijrmhm.2021.105693 (2021).

23. C. Jiang, H. Chen, Q. Wang, and Y. Li, *J. Mater. Process. Technol.* 229, 562 https://doi.org/10.1016/j.jmatprotec.2015.09.044 (2016).

24. V. Jankauskas, M. Antonov, V. Varnauskas, R. Skirkus, and D. Goljandin, *Wear* 328, 378 https://doi.org/10.1016/j.wear.2015.02.063 (2015).

25. H. Li, Y. Hu, R. Di, R. Yuan, C. Shi, and J. Lei, *Ceram. Int.* 48, 20388 https://doi.org/10.1016/j.ceramint.2022.03.324 (2022).

26. B. Cheniti, D. Miroud, R. Badji, D. Allou, T. Csanádi, M. Fides, and P. Hvizdoš, *Int. J. Refract. Met. H.* 64, 210 https://doi.org/10.1016/j.ijrmhm.2016.11.004 (2017).

27. M.N. Avettand-Fènoël, T. Nagaoka, H. Fujii, and R. Taillard, *J. Manuf. Process.* 40, 1 https://doi.org/10.1016/j.jmapro.2019.02.032 (2019).

28. T. Soria-Biurrun, L. Lozada-Cabezas, J. Navarrete-Cuadrado, F. Ibarreta-Lopez, R. Martinez-Pampliega, and J.M. Sánchez-Moreno, *Int. J. Refract. Met. H.* https://doi.org/10.1016/j.ijrmhm.2022.105994 (2023).

29. W. Kayser, S. van Kempen, A. Bezold, M. Boin, R. Wimpory, and C. Broeckmann, *Int. J. Refract. Met. H.* https://doi.org/10.1016/j.ijrmhm.2019.105003 (2019).

30. J.F. Zhu, L. Zhang, H.D. Zhang, Z.Q. Zhong, L. Zhou, and Y. Chen, *Int. J. Refract. Met. H.* https://doi.org/10.1016/j.ijrmhm.2017.11.014 (2018).

31. A. Nordgren, and A. Melander, *Powder. metal.* 31, 189 https://doi.org/10.1179/pom.1988.31.3.189 (1988).

32. N.I. Romanova, G.S. Kreimer, and V.I. Tumanov, *Sov. Powder. Metall. Met. C.* 13, 670 https://doi.org/10.1007/BF00798346 (1975).

33. I.J. Shon, I.K. Jeong, I.Y. Ko, J.M. Doh, and K.D. Woo, *Ceram. Int.* 35, 339 https://doi.org/10.1016/j.ceramint.2007.11.003 (2009).

34. L.L. Dong, C. Weng, L.T. Hou, Y.B. Liu, and Q.W. Luo, *J. Mater. Process. Technol.* 238, 325 https://doi.org/10.1016/j.jmatprotec.2016.07.041 (2016).

35. D.L. Jia, P. Yi, Y.C. Liu, J.W. Sun, S.B. Yue, and Q. Zhao, *Surf. Coat. Technol.* https://doi.org/10.1016/j.surfcoat.2020.126561 (2021).

36. Y.J. Du, J.T. Xiong, F. Jin, S.W. Li, L. Yuan, D. Feng, J.M. Shi, and J.L. Li, *Mater. Sci. Eng. A.* https://doi.org/10.1016/j.msea.2020.140610 (2021).

37. T. Soria-Biurrun, L. Lozada-Cabezas, F. Ibarreta-Lopez, R. Martinez-Pampliega, and J.M. Sanchez-Moreno, *Int. J. Refract. Met. H.* https://doi.org/10.1016/j.ijrmhm.2020.105317 (2020).

38. J.H. Lee, J.C. Oh, J.W. Park, H.C. Lee, and S. Lee, *ISIJ Int.* 41, 859 https://doi.org/10.2355/isijinternational.41.859 (2001).

39. C. Qian, K. Li, X.Y. Guo, B. Liu, Z.Y. Long, and Y. Liu, *J. Cent. South. Univ.* 27, 1146 https://doi.org/10.1007/s11771-020-4355-5 (2020).